Chapter 2: Continuum Mechanics Models and Development of VUMAT

2.1 Introduction

The finite element analysis of many sheet forming problems faces often difficulties due to the strongly non-linear material behavior including friction which makes convergence difficult in implicit finite element schemes. Such problems can be better addressed within the framework of explicit schemes (such as ABAQUS/Explicit) especially when coupled with a remeshing strategy. The library of ABAQUS contains several constitutive models including isotropic hardening model kinematic hardening model and combined hardening model. Unfortunately, the version available in ABAQUS is not versatile enough as a number of parameters are considered to be constant. This problem is addressed in ABAQUS/Standard with the used of field variables and user subroutine "USDFLD" which is not available in EXPLICIT.

For this reason, we developed a VUMAT user subroutine for the most general version of combined isotropic/ kinematic hardening model for ABAQUS/EXPLICIT. In this chapter, we firstly present a summary of the combined hardening model and its calibration, as well as an integration model for the model and then we propose the modification of combined hardening model to predict correctly the stress-strain curves with reverted load and its validation.

2.2 Constitutive Models

In this study, the program is written in modular form so that different material models can be added in the future. At the present time there are seven continuum material models, although the isothermal elastic/plastic model is the only continuum model described here.

The main assumption is that the strain rate is constant from time t_{n_1} to t_n. During each conjugate gradient iteration, the latest values of the kinematic quantities are used to update the stress. All material models are written in terms of the un-rotated Cauchy stress σ and the deformation rate d in the un-rotated configuration. When calculating linear elastic material response, Hooke's law is used. In a rate form, this is written as

$$\dot{\sigma} = \lambda trace(d)\delta + 2\mu d \tag{2.1}$$

where λ and μ are the elastic Lame material constants.

2.2.1 Basic Definitions and Assumptions

Some definitions and assumptions are outlined here. In Figure 2.1, which geometrically depicts the yield surface in deviatoric stress space, the back stress (the center of the yield surface) is defined by the tensor α. If σ is the current value of the stress, the deviatoric part of the current stress is

$$S = \sigma - \frac{1}{3} trace(\sigma)\delta \qquad (2.2)$$
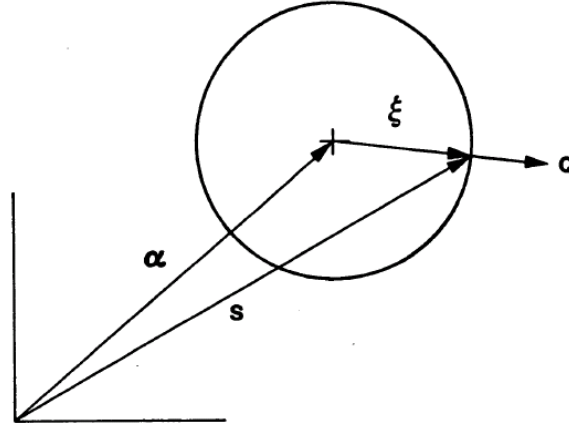
Figure 2.1: *Yield surface in deviatoric stress space.*

The stress difference is then measured by subtracting the backstress from the deviatoric stress by

$$\xi = S - \alpha \qquad (2.3)$$

The magnitude of the deviatoric stress difference R is defined by

$$R = \|\xi\| = \sqrt{\xi : \xi} \qquad (2.4)$$

where the inner product of second order tensors is $S : S = S_{ij}S_{jj}$. Note that if the back stress is zero (isotropic hardening case) the stress difference is equal to the deviatoric part of the current stress S.

The von Mises yield surface is defined as

$$f(\sigma) = \frac{1}{2}\xi : \xi = \kappa^2 \qquad (2.5)$$

and the von Mises effective stress is defined by

$$\bar{\sigma} = \sqrt{\frac{3}{2}\xi : \xi} \qquad (2.6)$$

Since R is the magnitude of the deviatoric stress tensor when $\alpha = 0$, it follows that

$$R = \sqrt{2}\kappa = \sqrt{\frac{2}{3}}\bar{\sigma} \tag{2.7}$$

The normal to the yield surface can be determined from Equation 2.5:

$$\boldsymbol{Q} = \frac{\partial f/\partial \sigma}{\|\partial f/\partial \sigma\|} = \frac{\xi}{R} \tag{2.8}$$

It is assumed that the strain rate can be decomposed into elastic and plastic parts by an additive decomposition,

$$d = d^{el} + d^{pl} \tag{2.9}$$

and that the plastic part of the strain rate is given by a normality condition,

$$d^{pl} = \gamma Q \tag{2.10}$$

where the scalar multiplier γ is to be determined.

A scalar measure of equivalent plastic strain rate is defined by

$$\bar{d}^{pl} = \sqrt{\frac{2}{3}d^{pl}:d^{pl}} \tag{2.11}$$

which is chosen such that

$$\bar{\sigma}\bar{d}^{pl} = \sigma : \Delta\,\varepsilon^{pl} \tag{2.12}$$

The stress is expressed in rate is assumed to be purely due to the elastic part of the strain rate and terms of Hooke's law by

$$\dot{\sigma} = \lambda trace(d^{el})\delta + 2\mu d^{el} \tag{2.13}$$

where λ and μ are the Lame constants for the material.

In what follows, the theory of isotropic hardening, kinematic hardening, and combined hardening is described.

2.2.2   Isotropic Hardening

In the isotropic hardening case, the back-stress is zero and the stress difference is equal to the deviatoric stress S. The consistency condition is written by taking the rate of Equation 2.5:

$$\dot{f}(\sigma) = 2\kappa\dot{\kappa} \tag{2.14}$$

The consistency condition requires that the state of stress must remain on the yield surface at all times. The chain rule and the definition of the normal to the yield surface given by Equation 2.8 is used to obtain

$$\dot{f}(\sigma) = \frac{\partial f}{\partial \sigma} : \dot{\sigma} = \left\| \frac{\partial f}{\partial \sigma} \right\| Q : \dot{\sigma} \tag{2.15}$$

and from Equations 2.4 and 2.5,

$$\left\| \frac{\partial f}{\partial \sigma} \right\| = \|S\| = R \tag{2.16}$$

Combining Equations 2.14, 2.15, and 2.16,

$$\frac{1}{R} S : \dot{\sigma} = \dot{R} \tag{2.17}$$

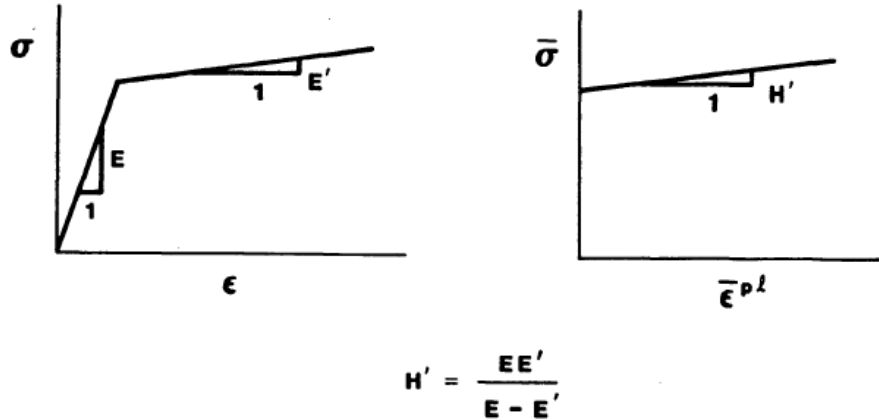Note that because S is deviatoric, $S : \dot{\sigma} = S : \dot{S}$, and

$$S : \dot{S} = \frac{d}{dt}\left(\frac{1}{2} S : S\right) = \frac{d}{dt}\left(\frac{\bar{\sigma}^2}{3}\right) = \frac{2}{3}\bar{\sigma}\dot{\sigma} \tag{2.18}$$

Then Equation 2.17 can be written as

$$\dot{R} = \sqrt{\frac{2}{3}}\dot{\bar{\sigma}} = \sqrt{\frac{2}{3}}H'\bar{d}^{pl} \tag{2.19}$$

where *H'* is the slope of the effective stress versus equivalent plastic strain ($\bar{\sigma}$ vs. $\bar{\varepsilon}^{pl}$). This may be derived from uniaxial tension test data as shown in Figure 2.2.

Figure 2.2: *Conversion of data from a uniaxial tension test to equivalent plastic strain versus von Mises stress.*

The consistency condition (Equation 2.17) and Equation 2.19 result in

$$\sqrt{\frac{2}{3}}H'\bar{d}^{pl} = Q:\dot{\sigma} \tag{2.20}$$

The trial elastic stress rate $\dot{\sigma}^{tr}$ is defined by

$$\dot{\sigma}^{tr} = C:d \tag{2.21}$$

where C is the fourth-order tensor of elastic coefficients defined by Equation 2.13. Combining the strain rate decomposition defined in Equation 2.9 with Equations 2.20 and 2.21 yields

$$\sqrt{\frac{2}{3}}H'\bar{d}^{pl} = Q:\dot{\sigma}^{tr} - Q:C:d^{pl} \tag{2.22}$$

Since Q is deviatoric, *C: Q = 2μQ and Q: C: Q = 2μ.* Then using the normality condition (Equation 2.10), the definition of equivalent plastic strain (Equation 2.11), and Equation 2.22,

$$\frac{2}{3}H'\gamma = Q:\dot{\sigma}^{tr} - 2\mu\gamma \tag{2.23}$$

and since Q is deviatoric ($Q:\dot{\sigma}^{tr} = 2\mu Q:d$), γ is determined from Equation 2.23 as

$$\gamma = \frac{1}{\left(1+\frac{H'}{3\mu}\right)}Q:d \tag{2.24}$$

The current normal to the yield surface Q and the total strain rate d are known quantities. Hence, from Equation 2.24, γ can be determined and then used in Equation 2.10 to calculate the plastic part of the strain rate. With the additive strain rate decomposition and the elastic stress rate of Equations 2.9 and 2.13, this completes the definition of the rate Equations.

The means of integrating the rate Equations, subject to the constraint that the stress must remain on the yield surface, still remains to be explained. How that is accomplished will be shown in Section 2.3.2.

2.2.3 Kinematic Hardening

For kinematic hardening, the von Mises yield condition is written in terms of the stress differenceξ:

$$f(\xi) = \frac{1}{2}\xi:\xi = \kappa^2 \tag{2.25}$$

It is important to remember that both ξ and the back stress α are deviatoric tensors.

The consistency condition for kinematic hardening is written as

$$\dot{f}(\xi) = 0 \tag{2.26}$$

because the size of the yield surface does not grow with kinematic hardening ($\dot{\kappa} = 0$). Using the chain rule on Equation 2.26, and

$$\frac{\partial f}{\partial \xi} : \dot{\xi} = 0 \tag{2.27}$$

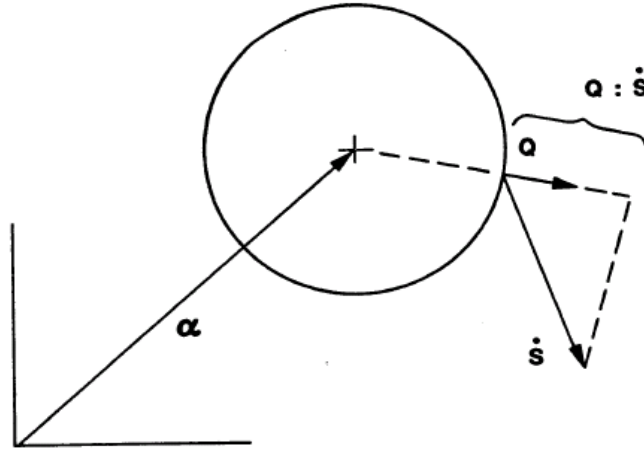$$\frac{\partial f}{\partial \xi} = \left\| \frac{\partial f}{\partial \xi} \right\| Q = RQ \tag{2.28}$$

Combining Equations 2.27 and 2.28 and assuming that R # 0,

$$Q : \dot{\xi} = 0 \tag{2.29}$$

or

$$Q :(\dot{S} - \dot{\alpha}) = 0 \tag{2.30}$$

A geometric interpretation of Equation 2.30 is shown in Figure 2.3 in which the back-stress moves in a direction parallel to the normal to the yield surface.

Figure 2.3: *Geometric interpretation of the consistency condition for kinematic hardening.*

The back-stress rate $\dot{\alpha}$ must now be defined. For the isotropic hardening case (Equation 2.20),

$$Q : \sigma = \sqrt{\frac{2}{3}} H' \bar{d}^{pl} = \frac{2}{3} H' \gamma \tag{2.31}$$

The kinematic hardening condition assumes that

$$\dot{\alpha} = \Phi d^{pl} = \Phi \gamma Q \tag{2.32}$$

where Φ is a material parameter. If Φ is chosen to be *(2/3) H'*, Equations 2.32 and 2.30 give a result identical to the isotropic hardening case (Equation 2.31). Hence, either Equation 2.31 or 2.32 gives us a scalar condition on $\dot{\alpha}$. Both of these are assumptions and must be shown to be reasonable. Experience with material models based on these assumptions has shown that, in fact, they are reasonable representations of material behavior.

Using Equation 2.32, Equation 2.9 (the strain rate decomposition), and Equation 2.13 (the elastic stress rate) in Equation 2.30 (the consistency condition for kinematic hardening) gives

$$Q : (\dot{\sigma}^{tr} - C : d^{pl}) = Q : \frac{2}{3} H' \gamma Q \tag{2.33}$$

Using the normality condition ($d^{pl} = \gamma Q$) and the fact that Q is deviatoric, $C:Q = 2\mu Q$. Solving Equation 2.33 for γ then gives

$$\gamma = \frac{1}{\left(1 + \frac{H'}{3\mu}\right)} Q : d \tag{2.34}$$

which is the same result as that of the isotropic hardening case.

2.2.4 Combined Isotropic and Kinematic Hardening

For the combined hardening case, a scalar parameter β is defined as ranging from 0 to 1, which determines the relative amount of each type of hardening. Figure 2.4 illustrates the uniaxial response to reversed loading that results from different choices of β. When $\beta = 0$, only kinematic hardening occurs, and when $\beta = 1$, only isotropic hardening occurs.
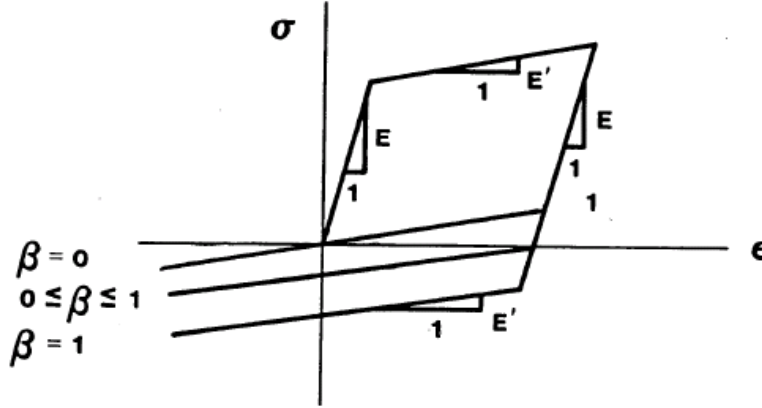
Figure 2.4: *Effect of the hardening parameter β on uni-axial response.*

The results derived for the independent hardening cases are multiplied by the appropriate fraction for each type of hardening. Equations 2.19 and 2.32 are rewritten as

$$R = \sqrt{\frac{2}{3}} H' \bar{d}^{pl} \beta \tag{2.35}$$

$$\dot{\alpha} = \frac{2}{3} H' d^{pl} (1 - \beta) = \frac{2}{3} H' \gamma Q (1 - \beta) \tag{2.36}$$

As before, the consistency condition is

$$Q : \dot{\xi} = \dot{R} \tag{2.37}$$

or

$$Q : (\dot{S} - \dot{\alpha}) = \sqrt{\frac{2}{3}} H' \bar{d}^{pl} \beta \tag{2.38}$$

Using the elastic stress rate, the additive strain rate decomposition, and the normality condition, $Q : \dot{S} = Q :(\dot{\sigma}^{tr} - \gamma C : Q)$ Together with Equations 2.36 and 2.11, this transforms Equation 2.38 into

$$Q : \dot{\sigma}^{tr} - \gamma Q : C : Q - \frac{2}{3} H' \gamma Q (1 - \beta) Q : Q = \sqrt{\frac{2}{3}} H' \beta \sqrt{\frac{2}{3} (\gamma Q) :(\gamma Q)} \quad \text{(2.39)}$$

Solving for γ,

$$\gamma = \frac{1}{\left(1 + \frac{H'}{3\mu}\right)} Q : d \qquad \text{(2.40)}$$

which is the same result as was obtained for each of the independent cases.

The following is a summary of the governing Equations for the combined theory:

$$\dot{\sigma} = C :(d - d^{pl}) = \dot{\sigma}^{tr} - 2\mu\gamma Q \qquad \text{(2.41)}$$

$$\dot{R} = \beta \sqrt{\frac{2}{3}} H' \bar{d}^{pl} = \beta \frac{2}{3} H' \gamma \qquad \text{(2.42)}$$

$$\dot{\alpha} = (1 - \beta) \frac{2}{3} H' d^{pl} \qquad \text{(2.43)}$$

$$d^{pl} = \begin{cases} 0 (elastic), & if \quad f(\xi) < \kappa^2 \\ \gamma Q(plastic), & if \quad f(\xi) \geq \kappa^2 \end{cases} \qquad \text{(2.44)}$$

$$\gamma = \frac{1}{\left(1 + \frac{H'}{3\mu}\right)} Q : d \qquad \text{(2.45)}$$

$$Q = \frac{\partial f / \partial \sigma}{\| \partial f / \partial \sigma \|} = \frac{\xi}{R} \qquad \text{(2.46)}$$

2.3   Implementation of Combined Hardening Law and Development of VUMAT

The constitutive model presented in the previous section was implemented in the ABAQUS, a general-purpose finite element program [32]. This code provides a general interface for user programmed constitutive models through a "user subroutine" (VUMAT for ABAQUS/Explicit). As discussed above, we develop our own user subroutine because the versions of hardening behavior models in ABAQUS/Explicit are not flexible enough. Figure 2.5 shows schematically the integration procedure in ABAQUS/Explicit with a VUMAT. For each time step, ABAQUS integrates the Equations of equilibriums based on the stress state at the beginning of the step at each integration point and provides the deformation gradient for VUMAT subroutine. VUMAT then finishes the integration of the constitutive model and updates the stress and state variable for each integration point. With the information that VUMAT provides, ABAQUS can then continue the calculation for the next time step.
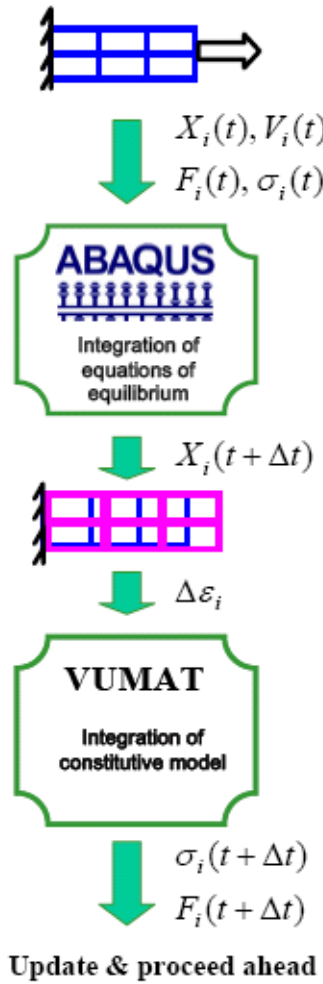
Figure 2.5: *ABAQUS and VUMAT subroutine.*

2.3.1   Derivation of the Constitutive Equations Elasticity

A basic assumption of elastic-plastic models is that the deformation can be divided into an elastic part and an inelastic (plastic) part. There are mainly two methods of decomposition of kinematics: (a) multiplicative decomposition $\mathbf{F} = \mathbf{F^{el}} \mathbf{F^{pl}}$, in which it requires that the plastic deformation gradient $\mathbf{F^{pl}}$ (9 elements) is stored as a state variable for all integration points. (b) additive decomposition: $\Delta\varepsilon = \Delta\varepsilon^{el} + \Delta\varepsilon^{pl}$ where $\Delta\varepsilon$ is the total strain increment, $\Delta\varepsilon^{el}$ is the increment of the elastic strain, and $\Delta\varepsilon^{pl}$ is the increment of inelastic strain. The additive decomposition is adequate when the elastic strains are small. For a linear and isotropic material:

$$\Delta\sigma = C\Delta\varepsilon^{el} = C(\Delta\varepsilon - \Delta\varepsilon^{pl}) \text{ with } C \equiv 2GI + (K - 2G/3)\delta : \delta \qquad (2.47)$$

where **C** is the forth order elasticity tensor, $\boldsymbol{I}$ and $\boldsymbol{\delta}$ are respectively the forth and second order identity tensor, G and K are the shear modulus and bulk modulus respectively which are

functions of powder porosity. For isotropic materials, $G = \dfrac{E}{2(1+\nu)}$ and $K = \dfrac{E}{3(1-2\nu)}$ where E and ν are Young's modulus and Poisson's ratio, respectively.

Plasticity: The evolution Equation for the plastic part of the deformation gradient ("flow rule") is given by $\Delta\bar{\varepsilon}^{pl} = \Delta\gamma Q$ where, $\Delta\gamma$ will be determined in Section 2.3.2. The details of time integration procedure are discussed below.

2.3.2   Integration procedure

For a typical time step, our VUMAT uses explicit Euler algorithm (Euler forward) to integrate stresses and internal state variable. The time increment is limited by the overall stability limit of the explicit integration of the Equations of motion. This is usually more restrictive than the stability limit of the stress integration in the VUMAT. Other integration algorithms are also can be used, such as implicit Euler algorithm (Euler backward) [33, 34] or semi-implicit Euler algorithm [35]. Since the stability constrain limits the overall time increment, explicit and semi-explicit methods (i.e. not iterative methods) are more efficient than fully implicit which are more appropriate for large time steps and plastic strain increments. The VUMAT uses the stress and internal variables at the beginning of an increment and the strain increment provided by ABAQUS and needs to predict the stress at the end of the increment, as well as the new values of the internal state variables.

The increment of strain across a time step $\Delta t = t_{n+1} - t_n$ is

$$\Delta\varepsilon_{n+1} = \Delta\varepsilon^{el}_{n+1} + \Delta\varepsilon^{pl}_{n+1} \tag{2.48}$$

The finite element algorithm requires an incremental form of Equations 2.41 through 2.46. Additionally, an algorithm must be used that integrates the incremental Equations subject to the constraint that the stress remains on the yield surface.

The incremental analogs of Equations 2.41 through 2.43 are

$$\sigma_{n+1} = \sigma^{tr}_{n+1} - 2\mu\Delta\gamma Q \tag{2.49}$$

$$R_{n+1} = R_n + \frac{2}{3}\beta H'\Delta\gamma \tag{2.50}$$

$$\alpha_{n+1} = \alpha_n + (1-\beta)\frac{2}{3}\Delta\gamma H'Q \tag{2.51}$$

where $\Delta\gamma$ represents the product of the time increment and the equivalent plastic strain rate ($\Delta\gamma = \gamma\Delta t$) The subscripts n and $n+1$ refer to the beginning and end of a time step, respectively; H, the slope of the uniaxial yield stress versus the plastic strain curve, is calculated by Equations (2.52), and β, the scalar parameter, is defined as ranging from 0 to 1. When $\beta =$

0, only kinematic hardening occurs, and when $\beta = 1$, only isotropic hardening occurs. For isotropic/kinematic hardening, β is determined by comparing cyclic tensile curves between experiment data and simulation data.

$$H = \frac{d\bar{\sigma}}{d\bar{\varepsilon}} = Kn\left(\varepsilon_0 + \bar{\varepsilon}_{pl}\right)^{n-1} \tag{2.52}$$

For nonlinear isotropic/kinematic hardening model, the size of yield surface was modified as a function of equivalent plastic strain $\bar{\varepsilon}_p$ and has the relationship with Swift's work-hardening law Equation (2.53) following Equation (2.54)
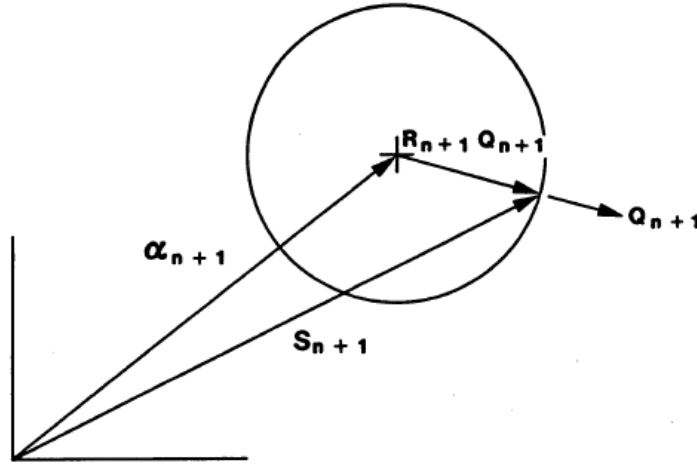
$$\bar{\sigma}(\bar{\varepsilon}_{pl}) = K(\varepsilon_0 + \bar{\varepsilon}_{pl})^n \rightleftarrows \tag{2.53}$$

$$\bar{\sigma}_Y(\bar{\varepsilon}_{pl}) = \bar{\sigma}(\bar{\varepsilon}_{pl}) - H\bar{\varepsilon}_{pl} \tag{2.54}$$

An incremental analog is needed for the rate forms of the consistency condition given by Equations 2.14, 2.26, and 2.38. At the end of the time step, the stress state must be on the yield surface. Hence, the incremental consistency condition is

$$\alpha_{n+1} + R_{n+1}Q = S_{n+1} \tag{2.55}$$

Equation 2.50 is depicted in Figure 2.6.

Figure 2.6: *Geometric interpretation of the incremental form of the consistency Condition for combined hardening.*

Substituting the definitions given by Equations 2.49 through 2.50 into the consistency condition of Equation 2.55,

$$\left[\alpha_n + (1-\beta)\frac{2}{3}H'\Delta\gamma Q\right] + \left[R_n + \frac{2}{3}\beta H'\Delta\gamma\right]Q = S_{n+1}^{tr} - 2\mu\Delta\gamma Q \tag{2.56}$$

Taking the tensor product of both sides of Equation 2.56 with Q and solving for $\Delta\gamma$,

$$\Delta\gamma = \frac{1}{2\mu} \frac{1}{\left(1+\frac{H'}{3\mu}\right)} \left(\|\xi^{tr}_{n+1}\| - R_n \right) \tag{2.57}$$

It follows from Equation 2.57 that the plastic strain increment is proportional to the magnitude of the excursion of the elastic trial stress past the yield surface (see Figure 2.6). Using the result of Equation 2.57 in Equations 2.49 through 2.51 completes the algorithm. In addition,

$$\Delta d^{pl} = \Delta\gamma Q \tag{2.58}$$

and

$$\Delta \bar{d}^{pl} = \sqrt{\frac{2}{3}} \Delta\gamma \tag{2.59}$$

Using Equation 2.57 in Equation 2.49 shows that the final stress is calculated by returning the elastic trial stress radially to the yield surface at the end of the time step (hence the name Radial Return Method). Estimates of the accuracy of this method and other methods for similarly integrating the rate Equations are available in Krieg and Krieg [28] and Schreyer et al. [29]. The radial return correction (the last term in Equation 2.49) is purely deviatoric. The summary of numerical integration algorithm of model is depicted in Figure 2.7.
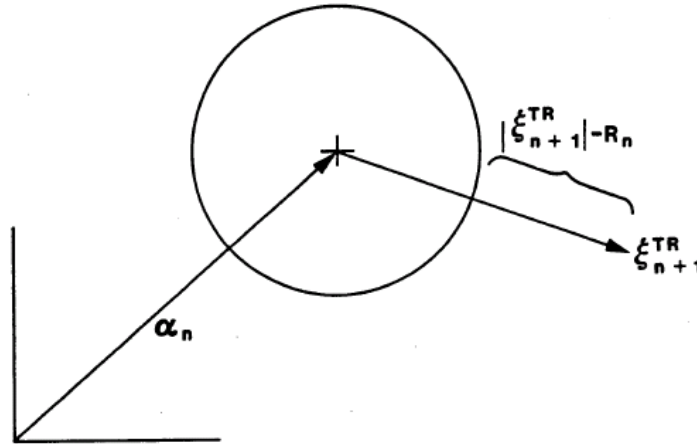

Figure 2.7: *Geometric interpretation of the radial returned correction.*

2.3.3   Verification of VUMAT subroutine

Above constitutive model is implemented into a commercial finite element program ABAQUS/Explicit via VUMAT user material for the uni-axial tension-compression and compression-tension tests with standard ASTM specimens for material of magnesium alloy

sheet which having rectangular cross-section of 13 mm width by 3.2 thickness and a gage length of 50 mm. in order to prevent buckling occurrence, a test method developed by Boger et al. [9], which relies on through-thickness sheet stabilization to avoid buckling, was used to extend the attainable strain range of Mg sheet in compression to approximately −0.08. A schematic of the novel tension/compression test [9] and the sample dimensions are shown in Figure 2.8 (a) two flat steel plates and a hydraulic cylinder system were used to provide side force to support the exaggerated dog-bone specimen. Side forces of 12 kN were used to stabilize the sheet sample. Figure 2.8 (b) shows the finite-element model of ABAQUS version 6.5 for test process. Here, the blank modeled using solid elements C3D8R, and the flat steel plate modeled using rigid surface-elements R3D4.


G = 36.8 mm, W = 15.2 mm
B = 50.8 mm, L > 3 mm
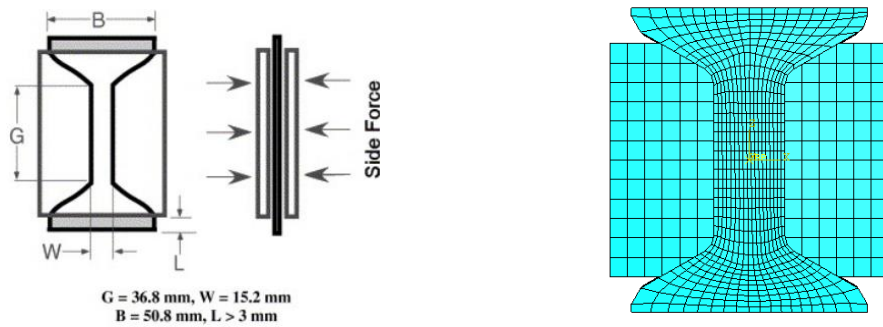
Figure 2.8: *Schematic of the novel tension/compression test [9]*

The average element size of the solid elements was about 1mm in width, 2mm in length, and 1mm in height. Meanwhile, the average element size of the rigid surface-elements was about 2 mm in width, and 2 mm in length. The friction coefficient μ at the blank/flat plate interface, μ_2=0.1, was assumed for all the simulations. The other material parameters are listed in Table 2.1.

Table 2.1: *Mechanical properties of tested material (Magnesium alloy sheet)*

Material	AZ31B
Density (r, kg/cm^3)	1.77e-06
Young's modulus (E, kN/cm^2)	45000
Possion's ratio	0.35
Tension yield stress (MPa) (σ_Y^T)	220
Compression yield stress (MPa) (σ_Y^C)	120
ε_0	0.005
K (MPa)	365.09
n	0.124

Figure 2.9 shows the comparisons between the FE simulation and experiment results. The best fit for uni-axial tensile test and Bauschinger effect was chosen with the scalar parameter β of 0.5. However, there are discrepancies between theoretical models and the test data in others zone. Therefore, in this chapter we have modified the hardening law to predict correctly behavior of stress-strain curves at reversed load for Mg alloy and also all others kind of materials.
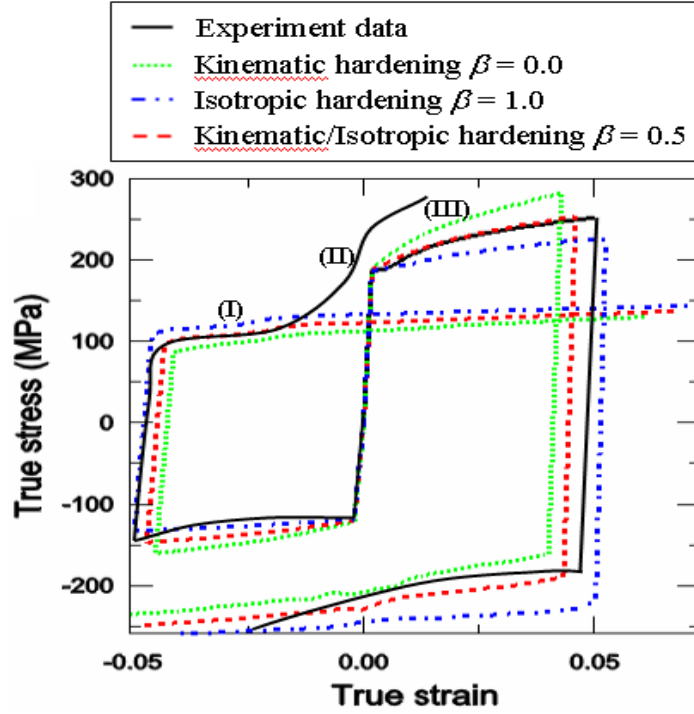
Figure 2.9: *The comparisons between the experiment result and FE simulation results of combined kinematic/isotropic hardening.*

2.3.4   A Modification of Combined Non-linear Hardening

As shown in Figure 2.9, when β changes from 0.0 to 1.0 the directions of cyclic tensile curves will be changed. It means that, if we can present β as a function of equivalent strain then we can predict correctly the shapes of stress-strain curves at compression and reversed stress. In this study, we proposed β as exponential function of equivalent strain. In compression stress, the scalar parameter β is expressed as below:

$$\beta^C = \beta_0 - F(\varepsilon^{pl(C)})^m \tag{2.60}$$

where β_0 is the initial direction of stress-strain curves when compression stress occurs. Here, $\beta_0 = 1$ is chosen to follow isotropic hardening direction. *F* and *m* are determined by fitting the generated curve from simulation with experiment data and chosen the best fit as *F* of 2.016e07 and *m* of 5 for Mg alloy sheet.

In case of reversed stress occurrence for compression-tension tests, as depict in Figure 2.9, the curve should be divided by three sections. The first section is formulated as Equation (2.61)

$$\beta_{R1}^{C-T} = \beta_0 - F_1(\varepsilon_R^{pl(C-T)})^{m1} \tag{2.61}$$

here, $\beta_0 = 1$, F_1 and m_1 was estimated as 1.952e08 and 5 for Mg alloy sheet, respectively. The second section is expressed as Equation (2.62) when $\varepsilon_R^{pl(C-T)}$ is greater than 0.04 mm.

$$\beta_{R2}^{C-T} = F_2(\varepsilon_R^{pl(C-T)})^{m2} \tag{2.62}$$

Similarly, F_2 and m_2 was estimated as 1.53e03 and 0.2 for Mg alloy sheet, respectively. The third section is generated when β_{R2}^{C-T} reaches $\beta = 0.5$ of fitting curve for uni-axial tensile test then $\beta_{R2}^{C-T} = 0.5$.

Figure 2.10 (a) shows the comparison of the measured continuous uni-axial tension-compression (T-C) and compression-tension (C–T) tests to the results calculated from the finite element simulations with proposed models. The results of proposed model are good agreement with measurements. Figure 2.10 (b) present the results of tension-compression (T-C) and compression-tension (C–T) FE simulation with various of pre-strain. To investigate this hardening model, finite element analysis of three-point bending-unbending test for the magnesium alloy sheet modeled using solid elements C3D8R is validated. The simulation results are depicted and plotted in Figure 2.11. In FE simulation result of three-point bending-unbending for solid elements, we can check tension-compression and compression-tension curves for correlative elements at the same time. The proposed hardening law simulates forward bending-unbending quite well comparing with tension-compression and compression-tension test in Figure 2.10

(a)   (b)
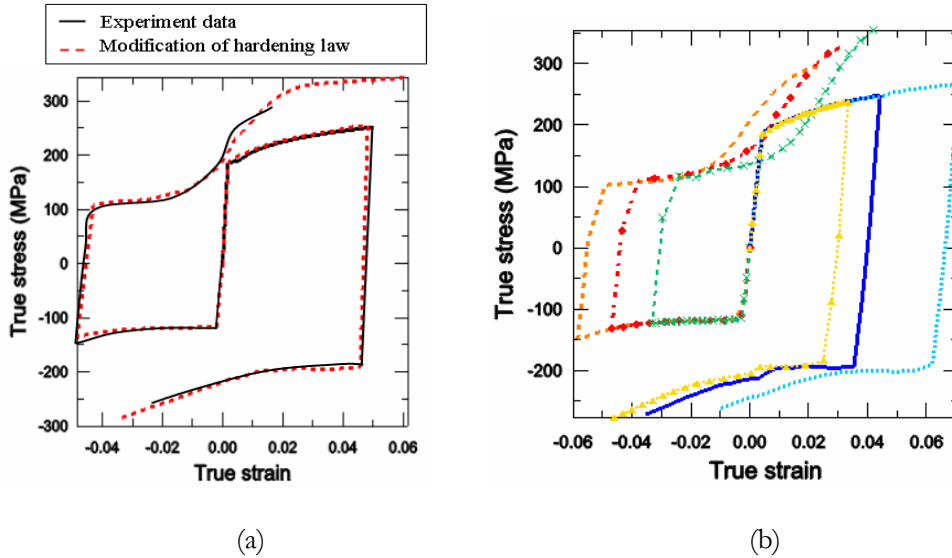
Figure 2.10: *Uni-axial tension-compression (T-C) and compression-tension (C–T) simulation results of proposed model comparing with experiment data (a) and with various of pre-strain (b)*
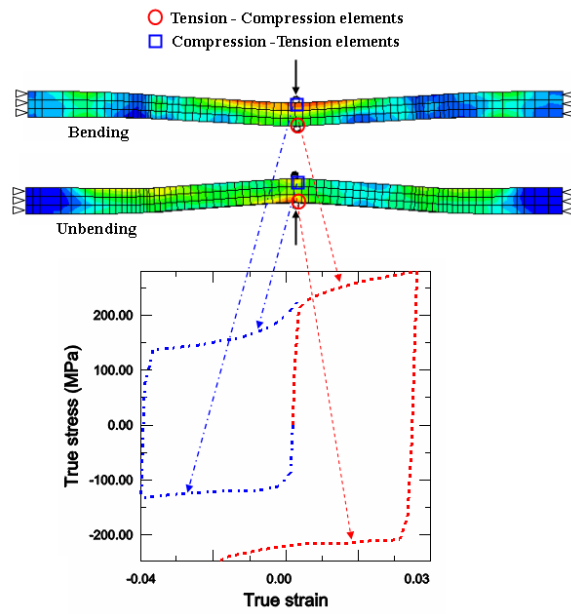
Figure 2.11: *FE simulation results for three-point bending-unbending process*